

## H-9-3

**Self-aligned MTJ etching technique using side walls for high-density 8F<sup>2</sup> MRAMs**

M. Yoshikawa<sup>1</sup>, M. Amano<sup>1</sup>, T. Ueda<sup>1</sup>, E. Kiatagawa<sup>1</sup>, S. Takahashi<sup>1</sup>, T. Kai<sup>1</sup>, T. Kishi<sup>1</sup>, N. Shimomura<sup>1</sup>, H. Aikawa<sup>1</sup>, T. Kajiyama<sup>2</sup>, K. Hosotani<sup>2</sup>, Y. Asao<sup>1</sup>, K. Suemitsu<sup>3</sup>, H. Hada<sup>3</sup>, S. Tahara<sup>3</sup>, and H. Yoda<sup>1</sup>

<sup>1</sup>Corporate Research & Development Center, Toshiba Corporation  
1, Komukai Toshiba-cho, Saiwai-ku, Kawasaki 212-8582, Japan

Phone: +81-44-549-2115, Fax: +81-44-520-1275, E-mail: masa.yoshikawa@toshiba.co.jp

<sup>2</sup>SoC Research & Development Center, Toshiba Corporation, Yokohama, Kanagawa 235-8522, Japan

<sup>3</sup>System Devices Research Laboratories, NEC Corporation, Sagami-hara, Kanagawa 229-1198, Japan

**1. Introduction**

Magnetoresistive random access memories (MRAMs) are based on the integration of magnetoresistive tunneling junctions (MTJs) and CMOS circuits and have the potential to compete with conventional semiconductor memories because of their nonvolatility, unlimited read/write endurance, higher operation speed and lower power consumption [1].

For high-density MRAMs, it is necessary to shrink a cell size. Recently, several new cell designs [2,3] with cell size of less than 8F<sup>2</sup> for cross-point and 1T+1MTJ MRAMs have been reported. However, those cells have some disadvantages such as complicated fabrication process and lower operating speed, compared with a conventional 1T+1MTJ MRAM cell. On the other hand, it is well known that magnetic switching fields are increased with the decrease of MTJ size, which causes the increase of write-operating currents. Therefore, in order to reduce a cell size, the minimization of several process margins is essential. In this paper, a modified 8F<sup>2</sup> cell design for 1T+1MTJ MRAMs is proposed, and a self-aligned (SA) MTJ fabrication process, which is a key to realize the 8F<sup>2</sup> cell, is developed and demonstrated. Finally, the influence of the SA MTJ fabrication process on magnetic and electrical properties is investigated.

**2. Cell design and process margin**

Figure 1 illustrates two types of cell designs for 1T+1MTJ MRAMs. Currently, a featured cell size is over 20F<sup>2</sup> in consideration of reasonable process margins and stable magnetic switching properties. If some process margins are omitted, the cell size is decreased to 12F<sup>2</sup> in Fig. 1 (a). Moreover, if the modified cell layout in Fig. 1 (b) is adopted, the cell size is reduced to 8F<sup>2</sup>. In both cases, an omission of a top electrode (TE)-bottom electrode (BE) process margin is essential. Additionally, a correlation between metal lines (M3, M4) and a MTJ and an accurate MTJ-ML alignment control are also important. On the other hand, a setting of a reasonable TE-BE space is critical to obtain large write-operating windows, because steep and large stray fields generated from pinned layers near the edges as shown in Fig. 2 cause large switching field distributions (SFDs), large offset fields, and asymmetry of astroid curves for conventional MRAMs [4]. Figure 3 shows the dependence of normalized SFDs and offset fields on free layer (FL)-pinned layer (PL) spaces. It is found that the reasonable FL-PL space of more than 50 nm, which

depends on pinned layer thickness, is required in order to obtain small offset fields and keep small SFDs in the case of 2.5 nm CoFe/Ru/2.5 nm CoFe synthetic antiferromagnetic (SAF) pinned layers.

**3. Self-aligned MTJ etch technique**

By using the SA MTJ etching process, it is possible to omit a TE-BE photolithography alignment margin and set a reasonable PL-FL space. Additionally, electrical shorts by the re-deposition across AlO<sub>x</sub> barriers are avoided. Figure 4 illustrates the process flow of the SA MTJ etching and Fig. 5 shows the top view SEM images after each fabrication process. The 1<sup>st</sup> step is the free layer etching stopped on the AlO<sub>x</sub> barriers using a 150 nm thickness hard mask (Fig. 4 (a)). The 2<sup>nd</sup> step is the side wall formation by a 100 nm SiO<sub>2</sub> deposition (Fig. 4 (b)) and a reactive ion etching (RIE) with a mainly C<sub>4</sub>F<sub>8</sub> chemistry (Fig. 4 (c)). Finally, the BE is etched by using the SiO<sub>2</sub> side wall as a mask (Fig. 4 (d)). In the SA process, the control of width and taper angle of the side wall, which depends on hard mask height, SiO<sub>2</sub> film coverage, and side wall forming RIE conditions, is critical to avoid strong stray fields generated from pinned layer edges and electrical shorts. Figure 6 shows a cross-sectional TEM image at a MTJ edge. The width and the taper angle of the side wall were precisely controlled to be around 50 nm and around 50 degrees, respectively.

**4. Electrical and magnetic properties**

The MTJs with a 0.24×0.48 μm<sup>2</sup> rectangular shape were composed of 4 nm NiFe free layers, 1 nm AlO<sub>x</sub> barriers, and 2.5 nm CoFe/Ru/2.5 nm CoFe SAF pinned layers. Figure 7 and 8 show the relationship between magnetoresistive ratio and resistance and astroid curves for different 3-types of MTJ etchings, respectively. No obvious electrical shorts were observed when the SA MTJ etching was used. In the case of the SA MTJ etching, the offset field of -7.5 Oe was slightly large, and some steps in the parallel to antiparallel switching at the easy axis direction as shown in Fig. 8 (a) were observed, which was caused by stray fields generated from the SAF pinned layers. These issues are settled by adjusting the SAF pinned layer thickness.

**5. Conclusions**

The SA MTJ fabrication process, which was a key technology to realize high-density 1T+1MTJ MRAMs with an 8F<sup>2</sup> cell design, was developed and demonstrated. In using the SA MTJ etching technique, no obvious electrical shorts were observed, and small SFDs and small offset

fields were obtained by a precise setting of the reasonable FL-PL space.

**Acknowledgements**

A portion of this work was supported by NEDO-F21.

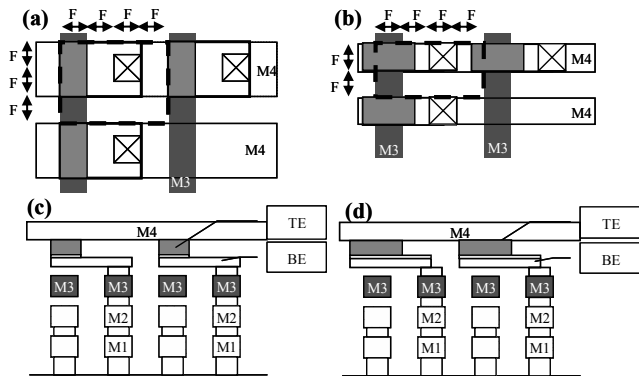


Fig. 1 Schematic illustrations of cell designs; (a) a top view and (c) a cross-sectional view of a conventional  $12F^2$  cell design with a  $2F^2$  MTJ, and (b) a top view and (d) a cross-sectional view of a modified  $8F^2$  cell design with a  $2F^2$  MTJ.

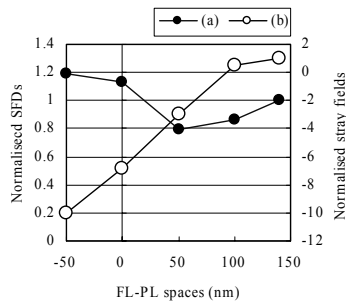


Fig. 3 Dependence of normalized SFDs (a) and offset fields (b) on FL-PL spaces of  $0.24 \times 0.48 \mu\text{m}^2$  rectangular MTJs with 2.5 nm CoFe/Ru/2.5 nm CoFe SAF pinned layers.

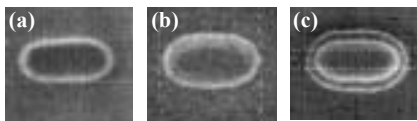


Fig. 5 Top view SEM images of  $0.24 \times 0.48 \mu\text{m}^2$  rectangular MTJs after TE etching (a), after side wall forming RIE (b), and after BE etching (c).

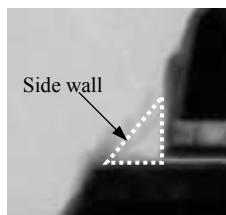


Fig. 6 Cross-sectional TEM image of a MTJ edge fabricated by the SA MTJ etching.

**References**

[1] S. Tehrani, *et al.*, IEEE Trans. Magn. 36 (2000) 2757  
 [2] Y. Asao *et al.*, IEDM Tech. Dig., (2004) 571  
 [3] J.H. Park *et al.*, IEDM Tech. Dig., (2003) 827  
 [4] M. Yoshikawa *et al.*, 49<sup>th</sup> Conference on MMM, (2004) GC-02

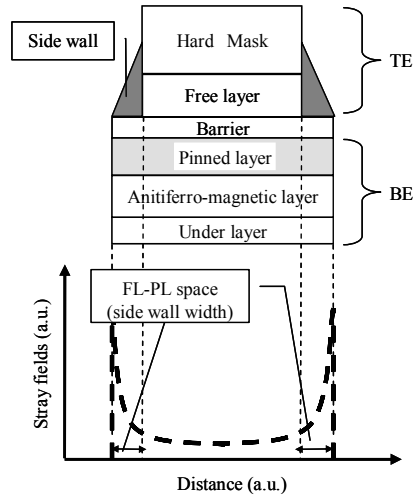


Fig. 2 Relationship between a schematic cross-sectional MTJ shape using the SA MTJ etching and a stray field distribution generated from pinned layers.

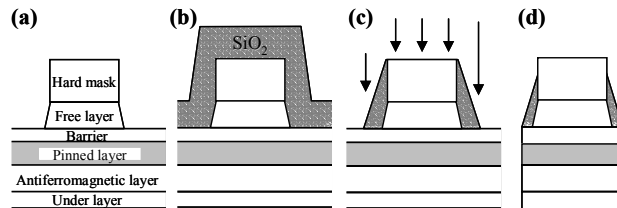


Fig. 4 Process flow of the SA MTJ fabrication. (a) TE etching, (b)  $\text{SiO}_2$  deposition, (c) side wall forming RIE, and (d) BE etching.

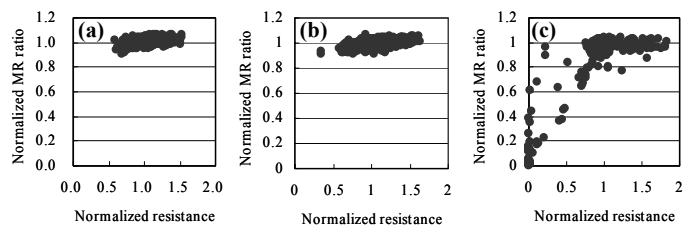


Fig. 7 Magnetoresistive ratio vs resistance of  $0.24 \times 0.48 \mu\text{m}^2$  rectangular MTJs in the case of (a) the SA MTJ etching, (b) the conventional 2-step MTJ etching, and (c) the conventional 1-step MTJ etching.

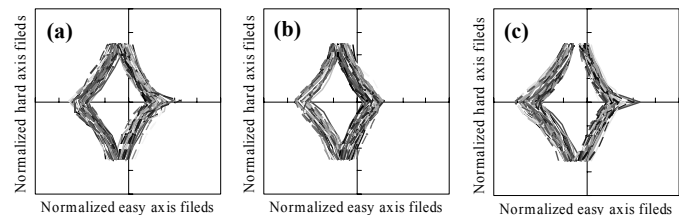


Fig. 8 Astroid curves of  $0.24 \times 0.48 \mu\text{m}^2$  rectangular MTJs in the case of (a) the SA MTJ etching, (b) the conventional 2-step MTJ etching, and (c) the conventional 1-step MTJ etching.